PAPER • **OPEN ACCESS**

Lunar accelerometer network gravitational observatory (LANGO)

To cite this article: Ho Jung Paik *et al* 2026 *Class. Quantum Grav.* **43** 095023

Classical and Quantum Gravity

PAPER

OPEN ACCESS

RECEIVED
20 November 2025

REVISED
24 April 2026

ACCEPTED FOR PUBLICATION
30 April 2026

PUBLISHED
14 May 2026

Lunar accelerometer network gravitational observatory (LANGO)

Ho Jung Paik[1,*], **Zachary Metzler**[2], **M Coleman Miller**[3], **Christopher J Collins**[4], **Clive R Neal**[5] and **Slava G Turyshev**[6]

[1] Department of Physics, University of Maryland, College Park, MD 20742, United States of America
[2] Chemistry Division, Los Alamos National Laboratory, Los Alamos, NM 87545, United States of America
[3] Department of Astronomy, University of Maryland, College Park, MD 20742, United States of America
[4] Institute of Photonics Technology, Aston University, Birmingham B47ET, United Kingdom
[5] Department of Civil and Environmental Engineering and Earth Sciences, University of Notre Dame, Notre Dame, IN 46556, United States of America
[6] Jet Propulsion Laboratory, California Institute of Technology, Pasadena, CA 91109, United States of America
[*] Author to whom any correspondence should be addressed.

E-mail: hpaik@umd.edu

Keywords: lunar gravitational-wave experiment, mid-frequency tensor gravitational-wave detector, LANGO, lunar accelerometers

Abstract

With ground-based interferometers detecting hundreds of gravitational-wave (GW) events, GW astronomy has continued to blossom. U.S. and European scientists are developing plans to construct third-generation ground-based interferometers. ESA has proceeded through the mission formulation phase of space-based interferometer in a lower-frequency band, 10^{-4}–0.1 Hz. Despite all these exciting developments, there is still a missing frequency band, 0.1–10 Hz. This mid-frequency band is rich with interesting astrophysical events. Coalescence and merger of intermediate-mass black holes (IMBHs) will occur in this frequency band. Coalescing stellar-mass BHs will pass through this frequency band days before they reach the frequency band of LIGO and Virgo. Detection of such signals would enable a mid-frequency detector to issue an advance notice to the high-frequency GW detectors, as well as to optical, x-ray and γ-ray telescopes. We propose Lunar Accelerometer Network Gravitational Observatory (LANGO) to detect GWs in this frequency band. In the first phase (LANGO 1), we propose to deploy four ambient-temperature (250 K) accelerometers in the tetrahedral or in a square configuration on the hemisphere facing the Earth. After successful operation at 250 K, LANGO would be upgraded to a cryogenic (4 K) version with over two orders of magnitude increased sensitivity (LANGO 2), with coherent rejection of seismic noise implemented. LANGO is a full-tensor detector, capable of determining the source direction and wave polarization. Each test mass (TM) is suspended as a pendulum with resonance frequency ~ 0.01 Hz, thus is only weakly coupled to the lunar surface horizontally. LANGO is designed to detect the relative motion of globally separated, nearly free, TMs by using the Moon as a large quiet platform. LANGO 1 and 2 accelerometers aim at sensitivities $\leqslant 10^{-11}$ m s^{-2} Hz$^{-1/2}$ and $\leqslant 10^{-13}$ m s^{-2} Hz$^{-1/2}$ in the horizontal axes over the frequency band of 1 mHz–10 Hz, which yield GW sensitivities 1.1×10^{-21} Hz$^{-1/2}$ and 3.8×10^{-24} Hz$^{-1/2}$ at 1 Hz, respectively. The LANGO accelerometers will be 10^3–10^5 times more sensitive than Apollo seismometers. With such sensitivity, LANGO will also make great contribution to the advancement of lunar geophysics.

1. Science objectives

Gravitational waves (GWs) offer a unique perspective on fundamental physics. The explosive coalescence of super compact objects such as black holes (BHs) and neutron stars (NSs) allows us to investigate the regime of extreme gravitational fields. These objects create highly curved, non-linear spacetime environments, which can be explored precisely by measuring the inspiral of compact objects. During the final merger and ringdown phase, these objects approach the speed of light, producing fields that are strong,

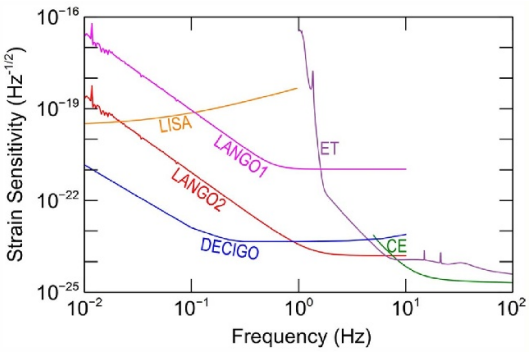

Figure 1. GW strain sensitivities of LANGO 1 and 2 compared to those of proposed ground and space interferometers.

nonlinear, and highly dynamical—a regime that is only now beginning to be explored by observations, and which can yield new tests of General Relativity (GR) and searches for physics beyond the Standard Model.

1.1. Gravitational-wave astronomy and test of theories of gravitation

The direct detection of GWs in 2015 by Advanced LIGO [1] began an era of GW astronomy, as well as for tests of GR. The addition of Advanced Virgo has enabled the detection and systematic study of dozens of GW signals from merging BHs and NSs, including the spectacular multi-messenger event GW170817 [2]. U.S. and European scientists are advancing plans to construct third-generation ground detectors, Cosmic Explorer (CE) [3] and Einstein Telescope (ET) [4]. ESA is formulating the LISA mission, with support from NASA, so that LISA could be observing in a lower-frequency band from late 2030s [5].

With all these exciting developments, there will still be a missing frequency band, 0.1–10 Hz, left between the ground and space interferometers. Many astronomical sources are expected to be in this frequency band, such as merging white dwarfs, NSs and intermediate-mass BHs (IMBHs), as well as type-1a supernovae [6, 7]. Further, mid-frequency detectors would detect coalescing stellar-mass BHs days before merging and could alert the GW detectors as well as optical, x-ray, γ-ray and neutrino astronomy communities, enabling more efficient multi-messenger astronomy [8].

We propose LANGO (Lunar Accelerometer Network Gravitational Observatory) to cover the frequency band of 0.1–10 Hz. In the first phase (LANGO 1), we propose to deploy 4 *ambient-temperature* (250 K) accelerometers in the tetrahedral or in a square configuration on the hemisphere facing the Earth (see section 2.1). After successful operation at 250 K, LANGO would be upgraded to a *cryogenic* (4 K) version with over two orders of magnitude increased sensitivity (LANGO 2). But the lunar seismic background would prevent such cryogenic accelerometers from operating at their full potential sensitivity [9]. In phase 1, we will measure the background seismic noise of the Moon and in phase 2, coherent rejection of seismic noise [10] would be implemented to suppress the seismic noise to the instrument noise level (see section 3.2).

Figure 1 shows the projected sensitivities of LANGO 1 and 2 compared to those of third-generation ground interferometers, CE and ET, as well as proposed space interferometers, LISA and DECIGO [11]. Although less sensitive than DECIGO below 1 Hz, LANGO would be serviceable whereas the other space detectors would not, have a longer lifetime, and also return lunar science. Some alternative theories of gravity predict the existence of scalar GWs [12]. By searching for a GW response of the monopole modes of the Moon, LANGO can directly test such theories of gravity.

1.2. Lunar geophysics and seismology

The seismicity in and on the Moon was defined by the Apollo Passive Seismic Experiment that returned data until 30 September 1977 from stations deployed by Apollo 12, 14, 15, and 16. Gravity data from the recent GRAIL mission were compared to the Apollo seismic data in order to determine the geological structure of the Moon (e.g. [13]). While the GRAIL gravity data are global, the seismic network covered a small area of the Moon on the central nearside making interpretations of the mid to deep lunar interior equivocal (see [14]). There is still much to learn about the lunar interior, which can be obtained from a network of highly sensitive broadband seismometers that are globally distributed. This forms the lunar geophysical network (LGN) concept that has been a named high priority New Frontiers mission in the last two planetary science decadal surveys [15, 16].

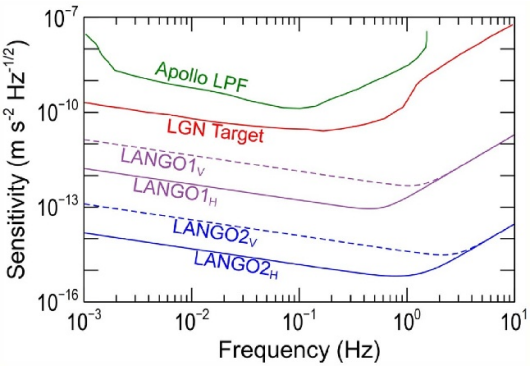

Figure 2. Sensitivities of LANGO 1 and 2 accelerometers compared to that of Apollo seismometers and LGN target sensitivity.

The increased sensitivity in detection is critical to measure the normal modes of the Moon (i.e., the natural, harmonic frequencies at which the Moon oscillates *after* a seismic event). As many of the moonquakes measured by the Apollo network were at the detection limits of seismometers, more sensitive detectors are necessary. Normal modes will give information about the size, composition, and density of the crust, mantle, and core. These modes will also help constrain the temperature, mineralogy, and fluid content of the mantle. Broadband seismometers with 1–2 orders of magnitude better sensitivity than the Apollo seismometers are under development to reach the LGN target sensitivity [17].

Since accelerometers measure the test mass (TM) displacements relative to the ground, the response of the Moon to GWs as well as to moonquakes and meteorite impacts must be measured or modeled in order to extract GW signals with high sensitivity. Hence, measurement and modeling of the Moon's eigenmodes from 1 mHz to 10 Hz would be necessary. GW detection and investigation of the lunar interior structure must go hand in hand, especially as the GW detectors could help in measuring the normal modes.

LANGO 1 and 2 accelerometers aim at sensitivities of $\leqslant 10^{-11}$ m s^{-2} Hz$^{-1/2}$ and $\leqslant 10^{-13}$ m s^{-2} Hz$^{-1/2}$ in the horizontal axes, and one order of magnitude less in the vertical axis, over a frequency band of 1 mHz–10 Hz, which represents 3–5 orders of magnitude improvement over the Apollo seismometers (see figure 2). Such an instrument would be a powerful new tool for lunar geophysics and planetary science, especially as they have the potential to measure the normal modes of the Moon. Several globally deployed LANGO accelerometers may be able to detect deep moonquakes occurring anywhere on the Moon, and make a significant contribution to the improvement of the lunar interior model.

2. Design concept of LANGO

2.1. Accelerometer network

We have investigated both an octahedral [18, 19] and a tetrahedral [20, 21] configuration of accelerometers on the Moon. Due to gravity bias, the vertical axis of the LANGO accelerometer is one order of magnitude less sensitive than the horizontal. Interestingly, the SOGRO-type octahedral configuration of 6 *horizontal-only* accelerometers fails to form a full-tensor detector, but the tetrahedral configuration of 4 horizontal accelerometers, does form a full-tensor detector.

Figure 3(a) shows the tetrahedral configuration of 4 accelerometers deployed on 4 of the 8 vertices of a cube inscribed in the Moon. Figure 3(b) shows an alternative arrangement of 4 accelerometers occupying the 4 vertices of the cube face facing the Earth. Either option yields the same GW strain sensitivity as shown in figure 1, and the antenna pattern shown in figure 4. The square configuration has the advantage of not requiring a relay satellite to communicate with the accelerometers on the back side of the Moon. If the budget permits, 4 more accelerometers could be added so that 8 accelerometers occupy all 8 vertices. This will improve the strain sensitivity by $\sqrt{2}$ and increase the instrument's capability to reject local non-gravitational noise sources.

As the sensitivity of each accelerometer is greater in the horizontal modes (see Section 2.2), it is primarily these which are used to extract GW signals. It should be noted, however, that the vertical response of the accelerometers will provide extra information in high signal-to-noise ratio (SNR) GW

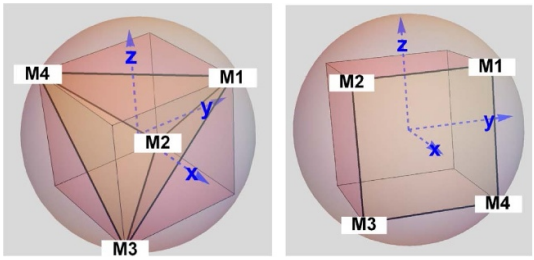

Figure 3. Four superconducting accelerometers deployed on the Moon (a) in a tetrahedral configuration and (b) in a square configuration.

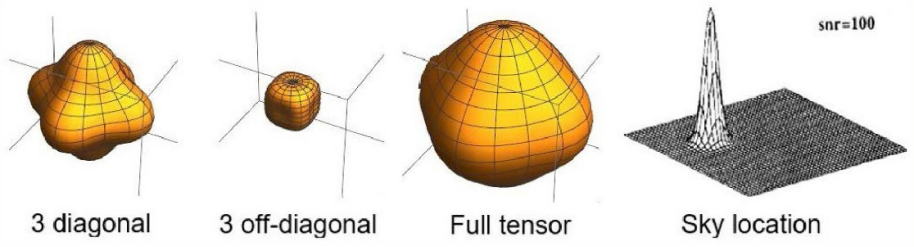

Figure 4. Antenna pattern of LANGO. As a full-tensor detector, LANGO has full-sky coverage with nearly equal sensitivity to waves coming from any direction with any polarization, and can locate the source in the sky.

signals, improving the overall GW detection sensitivity, as well as allowing tests of GR and providing a wealth of information about the lunar interior.

In order to most simply describe the geometry, we use a Cartesian coordinate system with origin at the center of the Moon, with the z axis passing through the north pole of the Moon. We then assume that the 4 accelerometers, M_1, M_2, M_3 and M_4, are placed at 4 of the 8 corners of an inscribed cube at the Moon's surface, at coordinates:

$$M_1 : \frac{R}{\sqrt{3}}(1,\ 1,\ 1), M_2 : \frac{R}{\sqrt{3}}(-1,\ 1, -1), M_3 : \frac{R}{\sqrt{3}}(1, -1, -1), M_4 : \frac{R}{\sqrt{3}}(-1, -1,\ 1) \tag{1}$$

where $R = 1737$ km is Moon's average radius. For the calculations in this section, we neglect the response of the Moon itself to the GWs. We will account for the effect of the response of the Moon in section 3. We can reconstruct the 6 GW tensor components h_{ij} by combining the horizontal outputs of the accelerometers in their respective local frames, as follows:

$$h_{xx} = \frac{\sqrt{3}}{2\sqrt{2}R\omega^2}(a_{1E} - a_{2E} - a_{3E} + a_{4E}) + \frac{1}{2\sqrt{2}R\omega^2}(a_{1N} - a_{2N} - a_{3N} + a_{4N}) \tag{2a}$$

$$h_{yy} = \frac{\sqrt{3}}{2\sqrt{2}R\omega^2}(-a_{1E} + a_{2E} + a_{3E} - a_{4E}) + \frac{1}{2\sqrt{2}R\omega^2}(a_{1N} - a_{2N} - a_{3N} + a_{4N}) \tag{2b}$$

$$h_{zz} = \frac{1}{\sqrt{2}R\omega^2}(-a_{1N} + a_{2N} + a_{3N} - a_{4N}) \tag{2c}$$

$$h_{xy} = \frac{1}{2\sqrt{2}R\omega^2}(a_{1N} + a_{2N} + a_{3N} + a_{4N}) \tag{2d}$$

$$h_{yz} = \frac{\sqrt{3}}{4\sqrt{2}R\omega^2}(-a_{1E} - a_{2E} + a_{3E} + a_{4E}) + \frac{1}{4\sqrt{2}R\omega^2}(-a_{1N} - a_{2N} + a_{3N} + a_{4N}) \tag{2e}$$

$$h_{zx} = \frac{\sqrt{3}}{4\sqrt{2}R\omega^2}(a_{1E} - a_{2E} + a_{3E} - a_{4E}) + \frac{1}{4\sqrt{2}R\omega^2}(-a_{1N} + a_{2N} - a_{3N} + a_{4N}) \tag{2f}$$

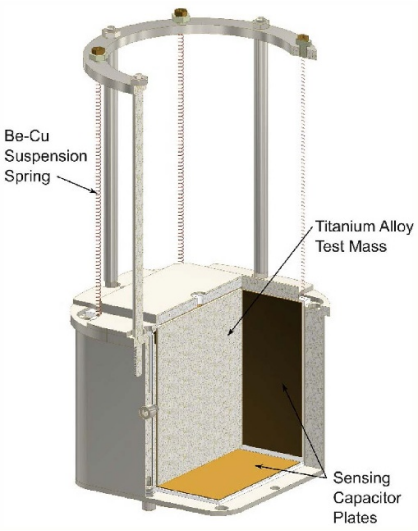

Figure 5. Cutaway view of LANGO-1 TM and housing.

where a_{ik} is the kth component of the horizontal linear acceleration of TM M_i, and E and N denote the local east and north direction, respectively. A detailed derivation of equation (2) is presented in appendix A. These equations show that the diagonal and off-diagonal h_{ij} components have the instrument-noise-limited sensitivity given by

$$S_{h,ii}(f) = \frac{2}{R^2\omega^4} S_a(f), S_{h,i\neq j}(f) = \frac{1}{2R^2\omega^4} S_a(f) \tag{3}$$

where $S_a(f)$ is the noise power spectral density (PSD) of each acceleration channel, which are assumed to be uncorrelated with one another. We will use equation (3) to compute the intrinsic detector noise of LANGO in section. 3.

Unlike the laser interferometer detectors, the Moon, instrumented with 4 accelerometers, has nearly uniform sky coverage (to $\leqslant$17%) with the unique capability of determining the sky location of the source and the polarization of the wave (see figure 4). Due to our use of only the horizontal components of the TM motion, the response to the off-diagonal components is reduced by a factor of 2 in amplitude compared to the diagonal components, resulting in the antenna pattern bulged along the 3 orthogonal axes.

2.2. Accelerometer design

LANGO-1 accelerometer described here is similar to the lunar seismometer demonstrated at the University of Maryland under NASA support [22]. LANGO-2 accelerometer is undergoing tests as part of technology development for a new GW detector called SOGRO with NSF support [18].

Figure 5 shows a cutaway view of LANGO-1 TM and its housing. The TM is made of Ti alloy Ti6Al4V and is supported by 4 beryllium–copper (Be–Cu) springs as a pendulum. The TM weighs $m = 5.0$ kg and the equilibrium length of the pendulum is $\ell = 0.25$ m. Under lunar gravity $g_M = 1.62$ m s^{-2}, the pendulum's natural frequency is

$$f_M = \frac{1}{2\pi}\sqrt{\frac{g_M}{\ell}} = 0.40 \text{ Hz} \tag{4}$$

The frequency is reduced to 0.01 Hz by applying electrostatic frequency reduction (EFR) [23]. In the vertical direction, the frequency is reduced from initial frequency 0.60 Hz to 0.03 Hz by EFR. Due to its higher resonance frequency, the vertical accelerometers will be less sensitive than the horizontal, but will still exceed the LGN target sensitivity (see figure 2). If buried under regolith of 1 m depth, the accelerometer would be at a stable temperature of 250 K [24]. Figure 6 shows LANGO-2 TM and its housing. It is made of brass with $m = 10$ kg and the frequency reduction is achieved by a superconducting negative spring [25]. A vertical degree of freedom could be added by replacing the suspension wires with springs as in LANGO 1. The TM carries a niobium (Nb) ring at its bottom for the negative spring. The LANGO-2 accelerometers require cooling to 4 K by cryocoolers.

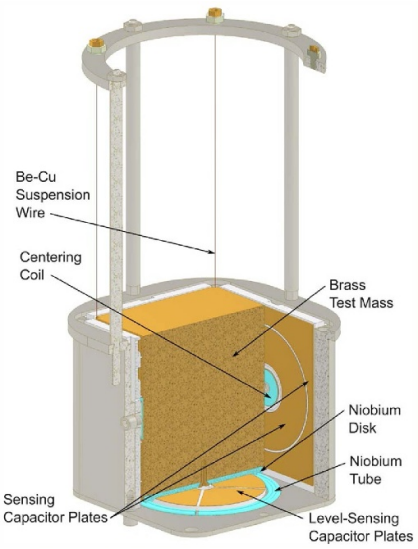

Figure 6. Cutaway view of LANGO-2 TM and housing.

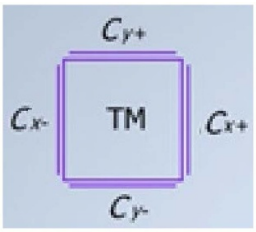

Figure 7. Configuration of sensing capacitors.

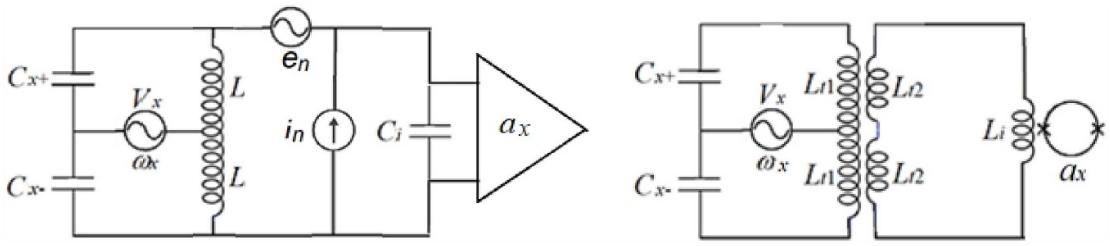

Figure 8. *LC*-bridge sensing circuits for (Left) LANGO 1 and (Right) LANGO 2.

Figure 7 shows the configuration of 4 sensing capacitors surrounding the TM in the horizontal plane. In addition, 2 capacitor plates (not shown) are located above and below the TM for vertical sensing. Figure 8 (left) shows the sensing circuit for LANGO 1 for acceleration component a_x. The two sensing capacitors, C_{x+} and C_{x-}, form an *LC* bridge with two coils with inductance L each. The bridge is coupled to a JFET preamplifier. The bridge is balanced by centering the TM. In LANGO 2, the *LC* bridge is coupled to a two-stage Magnicon SQUID (Superconducting Quantum Interference Device) with input energy resolution of $280\hbar$ at 4 K, as shown in figure 8 (right).

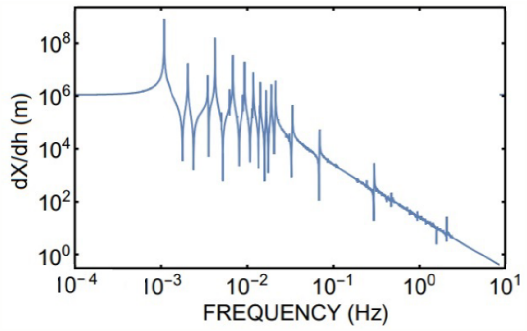

Figure 9. Moon's transfer function to a GW.

3. Strain sensitivity of LANGO

3.1. Intrinsic detector noise

Following Merkowitz and Johnson [26], we describe the Moon and the LANGO detector in the *laboratory frame*. The displacement vector of the lunar surface $\boldsymbol{u}$ is expanded as

$$u(\mathbf{x},\ t) = \sum_{\ell,m} a_{\ell m}(t)\, \boldsymbol{\Psi}_{\ell m}(\mathbf{x}) \tag{5}$$

where $\boldsymbol{\Psi}_{\ell m}(\mathbf{x})$ is the spatial eigenfunction given by

$$\boldsymbol{\Psi}_{\ell m}(\mathbf{x}) = [\alpha_\ell(r)\,\hat{r} + \beta_\ell(r)\,R\nabla]\, Y_{\ell m}(\theta,\phi)\,. \tag{6}$$

Here R is the radius of the Moon and $Y_{\ell m}(\theta,\phi)$ is the spherical harmonic. Only $\ell = 2$ modes couple to GWs, so we will drop the index ℓ for simplicity. The radial eigenfunctions are

$$\alpha(r) = cR\frac{\partial}{\partial r} j_2(qr) + 6\mathrm{d}R\frac{1}{r} j_2(kr)\,, \beta(r) = c j_2(qr) + \mathrm{d}\frac{\partial}{\partial r}[r j_2(kr)] \tag{7}$$

where j_2 is the spherical Bessel function of order 2, and q and k are the longitudinal and transverse wave vectors depending on Lamé coefficients λ and μ. The equation of motion can be written as

$$\ddot{a}_m(t) + \omega_m^2 a_m(t) = \frac{1}{\rho N_m}\int \mathrm{d}V \boldsymbol{\Psi}_m(\mathbf{x})\cdot f^{\mathrm{GW}}(\mathbf{x},t) \tag{8}$$

where ω_m is the resonance frequency of the mth mode of the Moon, $N_m = 4\pi R^3/3$, and $f_i^{\mathrm{GW}}(\mathbf{x},t) = \frac{1}{2}\rho\sum_j \frac{\partial^2 h_{ij}(t)}{\partial t^2} x_j$ is the force density exerted by a GW.

To compute the response of the Moon to a GW, we need to assume a lunar interior model. We then calculate its spectrum of elastic eigenmodes and the coupling of each of these modes to a GW, then use a weighted sum to determine the motion of the Moon's surface caused by the GW. Scattering by lunar regolith may further complete the analysis [27]. For simplicity, we approximate the Moon as *a sphere with uniform density and isotropic elastic properties*. The exact response of the Moon's surface is not important, as long as it is small compared the displacement of the TM with respect to the Moon's center, which is the case for LANGO, as will be shown below.

The computed transfer function of the Moon to a GW, $\mathrm{d}X/\mathrm{d}h$, is plotted in figure 9 from 10^{-4} to 10 Hz, where $X(f)$ is the *displacement of the lunar surface in frequency space* with respect to the unperturbed metric. The elastic parameters were chosen so that the fundamental quadrupole mode of the Moon becomes 1 mHz with $Q = 100$. The Moon's resonant response to a GW is clearly seen in the frequency band 1 mHz–0.03 Hz.

Although the GW sensitivity of LANGO in this frequency band would not be as good as at higher frequencies, detection of the Moon's quadrupole modes could serve a very important purpose for mid-frequency GW detection. To be able to determine the source direction and wave polarization and reject non-gravitational excitations to one part in 10^2, the sensitive axes of the 4 remotely deployed accelerometers must be aligned and the 8 acceleration channels must be cross-calibrated to the order of one part in 10^3. To accomplish this, we need a global excitation of the Moon. The response of quadrupole modes

of the Moon to meteorite impacts comes in handy and could just provide the calibration signals we need for LANGO.

In the mid-frequency band 0.1–10 Hz, the Moon's response drops to near zero, implying that the Moon acts as 'a rigid body' at these high frequencies, while the TM behaves as 'a free mass' since the TM resonance frequency is well below the signal frequency. The lunar transfer function plotted in figure 9 agrees with the lunar surface response computed by Yan *et al* [28] under similar assumptions. Figure 1 of [28] plots lunar response function T_h^A computed in the *transverse-traceless* gauge. As explained in the paper, T_h^A is the response to the *EM forces* induced by a GW (through its elastic modes), which is exactly what $\mathrm{d}X/\mathrm{d}h$ is.

In frequency space, the accelerometer response to a GW signal, $h(f)$, is given by

$$\left(\omega_0^2 - \omega^2 + \frac{j\omega\omega_0}{Q}\right)[x(f) - X(f)] = -\omega^2\left[\frac{1}{2}h(f)R_x - X(f)\right] \tag{9}$$

where ω_0 and Q are the *horizontal* resonance frequency and the quality factor of the TM, $x(f)$ and $X(f)$ are the *horizontal* displacements of the TM and the lunar surface with respect to the unperturbed metric, and R_x is the *horizontal* component of the position vector of the TM with respect to the center of the Moon. $X(f)$ has components coming from two different origins, a GW-driven component, which is coherent with $h(f)$, and a seismically driven component, which is incoherent with $h(f)$. Restricting ourselves to the GW-driven part, $X(f)$ can be written as $X_c(f) = \frac{\mathrm{d}X}{\mathrm{d}h}h(f)$. The Moon's tandem fall with the TM in the GW field reduces the effective radius of the Moon. However, according to figure 9, $\mathrm{d}X/\mathrm{d}h < 10^{-2}R$ at $f = 0.1$ Hz and $< 10^{-6}R$ at $f = 10$ Hz, therefore is negligible in the LANGO frequency band. Since $\omega_0 \ll \omega$ and $X(f) \ll \frac{1}{2}h(f)R_x$, we find

$$x(f) - X(f) = -\frac{\omega^2}{\omega_0^2 - \omega^2 + \frac{j\omega\omega_0}{Q}}\left[\frac{1}{2}h(f)R_x - X(f)\right] \approx \frac{1}{2}h(f)R_x. \tag{10}$$

Thus, the LANGO TMs respond to GWs as *nearly free masses* in the respective horizontal planes. In other words, the LANGO TMs are almost completely decoupled from the Moon in the horizontal planes and are accelerated only by the GW driving force. Therefore, with global deployment of multiple accelerometers, LANGO becomes a very sensitive mid-frequency GW detector.

The intrinsic instrument noise PSD of an accelerometer is given [18] by

$$S_{\mathrm{a}}(f) = \frac{4}{m}\left[k_{\mathrm{B}}TH(f) + \frac{|\omega^2 - \omega_0^2|}{\omega_{\mathrm{p}}}\left(1 + \frac{1}{\beta^2}\right)^{1/2}k_{\mathrm{B}}T_{\mathrm{N}}\right] \tag{11}$$

where $H(f)$ is the damping coefficient of the TM suspension, ω_{p} is the driving frequency of the rf pump oscillator, T_{N} is the amplifier noise temperature, and β is the energy coupling constant of the transducer. The gravitational, electrostatic and superconducting negative spring forces acting on the TM are all frictionless. Damping occurs only in the suspension wire, which undergoes bending. For the wire suspension, $H(f)$ is given [23] by

$$H(f) = \frac{\omega_M^2\,\phi(f)}{\omega} = \frac{\omega_M^2\,\eta\phi_{mat}(f)}{\omega} \tag{12}$$

where $\phi(f)$ is the internal loss angle of the suspension spring, and ω_M is the TM resonance frequency *before* a negative spring is applied. However, since bending is restricted to a small region near the pivot, $\phi(f)$ is *diluted* from the material loss angle $\phi_{\mathrm{mat}}(f)$ by a factor $\eta \ll 1$ [29].

Substituting equation (12) into equation (11), we find

$$S_{\mathrm{a}}(f) = \frac{4}{m}\left[\frac{k_{\mathrm{B}}T\omega_{\mathrm{M}}^2\phi(f)}{\omega} + \frac{|\omega^2 - \omega_0^2|}{\omega_{\mathrm{p}}}\left(1 + \frac{1}{\beta^2}\right)^{1/2}k_{\mathrm{B}}T_{\mathrm{N}}\right]. \tag{13}$$

For derivation of T_{N}, see Appendices B and C. β can be shown [18] to be

$$\beta = \frac{CE_{\mathrm{p}}^2Q_{\mathrm{p}}}{m|\omega^2 - \omega_0^2|}\left[1 + \left(2Q_{\mathrm{p}}\frac{\omega}{\omega_{\mathrm{p}}}\right)^2\right]^{-1/2}. \tag{14}$$

Table 1. Values of accelerometer parameters. Some are fixed by design and others are derived.

Accelerometer parameter	LANGO 1	LANGO 2
Mass of TM, m	5.0 kg	10 kg
TM resonance frequency, f_0	0.01 Hz	0.01 Hz
TM spring loss angle, $\phi\ (f)$	10^{-6}	10^{-8}
TM temperature, T	250 K	4.2 K
LC-bridge driving frequency, f_p	94 kHz	2.7 MHz
Sensing capacitance, C	100 pF	100 pF
Driving electric field, E_p	10^5 V m^{-1}	10^5 V m^{-1}
Quality factor of LC-bridge, Q_p	20	10^3
Bridge inductor, L	25 mH	—
Transformer primary, L_{t1}	—	20 μH
Transformer secondary, L_{t2}	—	5.0 μH
Transformer coupling, k^2	—	0.80
Transducer energy coupling, β	$(0.32\ \mathrm{Hz}/f)^2$	$(1.6\ \mathrm{Hz}/f)^2$
Amplifier noise temperature, T_N	5.2 K	0.017 K

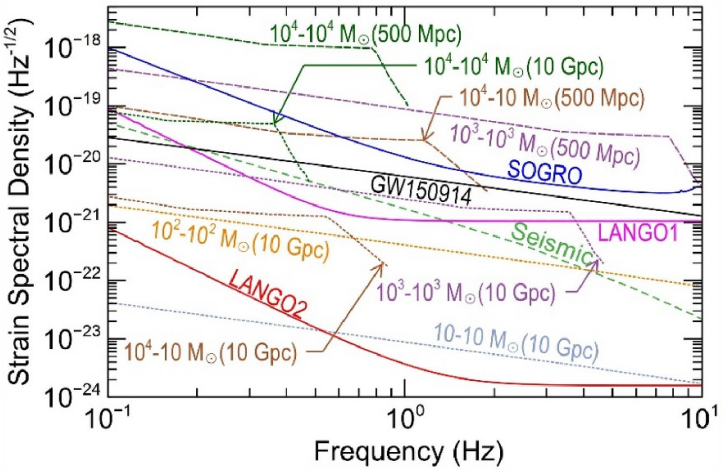

Figure 10. GW signals from IMBH binaries with various mass ratios at 500 Mpc and 10 Gpc, as well as the combined sensitivities of SOGRO and LANGOs. Also plotted is the signal from GW150914 in its coalescing phase.

The GW intrinsic detector noise PSD *combined over 5 independent tensor channels* can be obtained [30] from

$$\frac{1}{S_{h,\Sigma}(f)} = \sum_{i,j} \frac{1}{S_{h,ij}(f)}. \tag{15}$$

Substituting equation (3) into equation (15), and combining it with equation (13), we find

$$S_{h,\Sigma}(f) = \frac{1}{7R^2\omega^4} S_a(f) = \frac{4}{7mR^2\omega^4}\left[\frac{k_\mathrm{B}T\omega_M^2\phi(f)}{\omega} + \frac{|\omega^2-\omega_0^2|}{\omega_\mathrm{p}}\left(1+\frac{1}{\beta^2}\right)^{1/2} k_\mathrm{B}T_N\right] \tag{16}$$

where we included the projection of the GW driving forces to the horizontal plane.

Table 1 shows the design values of accelerometer parameters. For TM suspension, we could use a 0.38-mm diameter Be-Cu wire, whose yield strength has a safety margin of 500% in Earth's gravity. This wire gives a dilution factor of $\eta = 0.005$. At 300 K, Be-Cu shows $\phi_\mathrm{mat} = 5\times10^{-5}$ at 1 Hz [31], which gives $\phi = 2.5\times10^{-7}$. At 4 K, losses are typically reduced by two orders of magnitude. We assumed conservative values $\phi(f) = 10^{-6}$ and 10^{-8} for LANGO 1 and 2, respectively. Substituting them into equation (13), we find $S_a^{1/2}(1\ \mathrm{Hz}) = 2.0\times10^{-13}$ m s^{-2} Hz$^{-1/2}$ for LANGO 1 and 6.8×10^{-16} m s^{-2} Hz$^{-1/2}$ for LANGO 2. With baseline $L = \frac{2}{\sqrt{3}}R = 2.01\times10^6$ m, we obtain from equation (16) $S_{h,\Sigma}^{1/2}(1\ \mathrm{Hz}) = 1.1\times10^{-21}$ Hz$^{-1/2}$ for LANGO 1 and 3.8×10^{-24} Hz$^{-1/2}$ for LANGO 2.

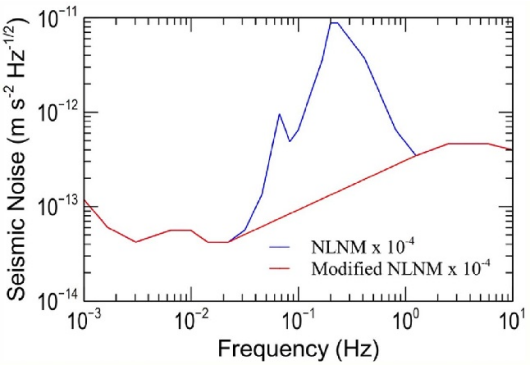

Figure 11. Estimated lunar background seismic acceleration noise level (red).

Figure 10 shows the GW signals from IMBH binaries with various mass ratios at luminosity distances 500 Mpc and 10 Gpc, and of the stellar-mass BH binary GW150914 ($36M_\odot$ -$29M_\odot$ at 410 Mpc), which was observed at higher frequencies by Advanced LIGO detectors. Also shown are the combined strain sensitivities of SOGRO and LANGO 1 and 2. With L increased from 50 m to 2,000 km, the sensitivity of LANGO 2 exceeds that of SOGRO [18] by over 3 orders of magnitude. The seismic noise limit computed in section 3.2 is plotted in green. LANGO 1 would be able to detect IMBH binaries to 10 Gpc, as well as coalescing stellar-mass BH binaries of the GW150914 size, giving an early warning for high-frequency detectors. Assuming a successful rejection of the seismic noise, LANGO 2 would extend the IMBH observation to beyond 10 Gpc and detect coalescing stellar-mass BH binaries with SNR $\geqslant 10^3$.

In GR, GWs couple only to the spheroidal quadrupole modes with $m = \pm 2$ of the Moon. The 8 horizontal acceleration outputs overdetermine the Moon's response to GWs. The extra degrees of freedom can be used to veto non-GW events such as those due to seismic motion of the Moon (except for random seismic noise background) or electromagnetic disturbances. The degree of discrimination between GW signals and local disturbances and the precision of source location and wave polarization depend on the sensitive axis alignment and the SNR. Numerical simulation to determine the precision of the recovered GW parameters from the axis misalignment and the accelerometer noise is beyond the scope of this paper.

3.2. Seismic noise

The random seismic noise background of the Moon has not been measured yet since it is below the sensitivity floor of the Apollo seismometers. It may require the full sensitivity of the LANGO-1 accelerometers to measure it. According to Lognonne *et al* [9], meteorite impacts generate seismic background noise on the Moon. They estimate the seismic background at 0.5 Hz to be *at least* 10^3 *times lower* than the new low noise model (NLNM) of the Earth [32].

Earth's NLNM exhibits a large microseism peak due to ocean waves. We remove this peak from NLNM in the 0.03–1 Hz frequency band, and then multiply 10^{-4} to obtain an estimated background seismic noise level of the Moon, which is plotted in figure 11. At 1 Hz, we get 3×10^{-13} m s^{-2} Hz$^{-1/2}$. This corresponds to strain noise $S_{h,\Sigma}^{1/2}(1\text{ Hz}) = 1.7 \times 10^{-21}$ Hz$^{-1/2}$, which is 450 times above the intrinsic noise of LANGO 2, as shown in figure 10. This would limit LANGO's reach for some lower-mass binary BH mergers to luminosity distances less than 10 Gpc, but will still allow many signals to be detected at great distances.

Transient seismic noise from moonquakes or impacts, being localized, will generally present a signature in the LANGO *network* which is clearly inconsistent with a GW. Thus, matched filtering which combines and compares all of the sensors in the network will be able to select GW signals. Random, continuous seismic noise effectively adds to the incoherent noise in the individual accelerometers. LANGO 2 requires 4 K cryocoolers. To avoid increasing the seismic noise, exported vibration from the cryocooler must be $< 3 \times 10^{-13}$ m s^{-2} Hz$^{-1/2}$ at 1 Hz. Although it will increase the cost of the LANGO mission, the random seismic noise could be cancelled to below the intrinsic noise level of LANGO by performing a *coherent noise cancellation* with an array of accelerometers in the vicinity of each TM [10].

For example, we could deploy 8 additional LANGO accelerometers on a ring of 5 km radius around each TM, as was illustrated in [33]. The GW sensitivity would increase by a factor of 3 on account of using 9 TMs per site, with the seismic noise reduced to below that level. Coherent seismic noise cancellation by a factor of 10^3 would be required to reach the full sensitivity of LANGO 2.

3.3. Justification for lunar experiment

LANGO is a far advanced version of the lunar gravimeter experiment that Weber attempted in the 1970's [34] and is an extension of the lunar GW experiments proposed by Paik and Venkateswara [35] and Harms *et al* [36].

Spherical resonant-mass GW detectors were proposed decades ago [37], and prototypes constructed and tested by a number of groups [38–40]. Although the spherical antenna has many advantages over the Weber-bar antenna, its development efforts were ultimately discontinued because, with the maximum diameter of ∼3 m that could be cast with aluminum, its sensitivity could not compete with long-baseline laser interferometers. Even SOGRO, which is a 'spherical' antenna with split TMs maintaining spherical symmetry, suffers from its limited baseline of 50 m due to the engineering challenge of constructing a larger platform with sufficient rigidity. *Here comes the Moon!* The Moon has 10^5–10^6 times the diameter of these antennas, and with the absence of plate tectonics, oceans and winds, its seismic background may be 10^4–10^5 times quieter than Earth. Therefore, with proper instrumentation, the Moon could become an ideal GW observatory. Unlike space interferometers, LANGO could be operational for $\geqslant$20 years.

While approximating the Moon as a sphere with uniform density and isotropic elastic properties may be appropriate for modeling the lunar response to GWs, it is not adequate for understanding lunar seismicity. The lunar megaregolith has been shown to scatter seismic energy, particularly in the records of shallow events (0–220 km) [41], and at frequencies above 2 Hz (e.g. [42],). However, the thickness of the megaregolith has been debated to be between ∼100 km [43] and 10–20 km (at least beneath the Apollo 12 site) [44]. The scattering effect via the megaregolith has important implications for defining epicenters for shallow moonquakes, the largest magnitude seismic events on the Moon [45]. Understanding the exact locations and magnitudes of such events has important implications for human space exploration of the Moon. Therefore, the ability to understand the normal modes for the Moon will be critical [27].

LANGO would be an excellent supplement to the LGN mission [17]. LGN proposes to distribute 4 landers around the Moon, with each lander containing laser retroreflectors, seismometers, electromagnetic sounders, and heat flow probes. The plan is to have each lander gather data continuously for 6 years with a goal of 10 years. The primary goal of LGN is to *understand the initial stages of terrestrial planet evolution*. If the LANGO network is active simultaneously with LGN, both missions would benefit each other. LANGO would yield data that would add fidelity to LGN. Conversely, LGN would inform LANGO regarding the detected signals—are they internal to the Moon or induced by meteoroid impact or other external sources? With the capability to observe the normal modes of the Moon, LANGO could also help improve the lunar interior model.

4. LANGO mission description

4.1. Deployment of accelerometers

Following a two-week cruise, when the spacecraft arrives at the Moon, propulsive maneuvers will place it into a nearly circular low lunar orbit. The 4 accelerometers are deployed pairwise from 2 different lunar orbits using the same lunar transfer stage. Once the first pair of spacecrafts with accelerometers is deployed, the stage changes its inclination to deploy the second pair. Landing on the Moon will be done autonomously using onboard landing capabilities.

4.2. Flight systems

The LANGO spacecraft includes all equipment necessary to deliver and support four 3-axis accelerometers on the Moon. The mass by subsystem is ∼200 kg. Attitude control will be done by using thrusters since there is no stringent pointing requirement for the spacecraft. Propulsion will be done by using a monopropellant to minimize cost of tanks and thrusters. The command and data handling subsystem is based on a standard architecture used for the lunar landers. Telecommunications will utilize standard X-band transponders and traveling-wave tube amplifiers with a deployed pointable high-gain antenna of 0.5 m diameter for sending instrument data to Earth.

4.3. Mission operations

Science operations of the LANGO accelerometers will be done on a continuous basis. The data will be stored onboard to communicate back to Earth. The spacecraft will have 3 view periods each day to select for operations. The tracking pass time will be selected to accommodate available tracking stations for that day. Once per week the spacecraft will communicate with a dedicated ground-based receiver network to download the science data from the previous week.

5. Conclusions

The Moon, with its low-noise environment, provides a unique opportunity to deploy a GW observatory capable of harnessing the information encoded within GWs to probe fundamental physics from an entirely new perspective. This new observatory will allow us to test Einstein's GR in previously inaccessible regimes by considering inspiral and merger-ringdown GW signals. In particular, analysis of compact-binary GW signals with LANGO will enable precision tests of gravitation by coherently combining high-SNR measurements of the mid-frequency band inspiral (0.1–10 Hz)—a frequency gap between ground and space interferometers—with the late inspiral/merger/ringdown observed by ground-based detectors at approximately 10 Hz and above, and with complementary low-frequency information where available. The mid-frequency band is particularly rich in IMBH binaries and in the early inspiral of stellar-mass binaries days prior to merger, enabling advance alerts and coordinated multiband and multi-messenger observing campaigns.

In this paper, we presented the designs and operating principles of LANGO 1 and 2, each constructed with 4 accelerometers in a tetrahedral (or square) configuration. We also described the procedure of reconstructing the 6 GW tensor components h_{ij} by combining the horizontal outputs a_{ik} of the 4 accelerometers in their respective local coordinate systems. We then derived the GW sensitivity of LANGO 1 and 2. With the baseline design parameters, the detector strain noise at 1 Hz, combined over 5 tensor components, is approximately 1.1×10^{-21} $\mathrm{Hz}^{-1/2}$ for LANGO 1 and 3.8×10^{-24} $\mathrm{Hz}^{-1/2}$ for LANGO 2, implying IMBH detection out to $\sim$10 Gpc with LANGO 1 and beyond 10 Gpc with LANGO 2 under successful seismic-noise rejection, and stellar-mass binary detections with SNR $\geqslant 10^3$ for LANGO 2. Unlike space interferometers, a lunar surface network can plausibly operate for 20+ years. Finally, beyond the standard quadrupolar response in GR, LANGO provides a direct search channel for scalar GW polarizations predicted by some alternative theories by targeting a GW response in the Moon's monopole modes.

In parallel, LANGO targets horizontal acceleration sensitivities $\leqslant 10^{-11}$ and 10^{-13} m s^{-2} $\mathrm{Hz}^{-1/2}$ for LANGO 1 and 2 over 1 mHz–10 Hz, corresponding to a 3–5 orders of magnitude improvement over Apollo-era seismometry and enabling sustained recovery of lunar eigenmodes and interior structure. Several globally deployed LANGO accelerometers may be able to detect deep moonquakes occurring anywhere on the Moon, and make a significant contribution to the improvement of the lunar interior model.

Acknowledgments

We acknowledge useful discussions with Vol Moody (in memory), Ronald Norton, Peter Shawhan, Ted Jacobson and Xian Chen. This work was partly supported by NSF Grants PHY1912627 and PHY2207757, and NASA Grant 80NSSC19K0447 and a NASA MatISSE program through Jet Propulsion Laboratory.

Data availability statement

No new data were created or analysed in this study.

Author contributions

Ho Jung Paik 0000-0001-8303-4529

Conceptualization (lead), Data curation (supporting), Formal analysis (lead), Funding acquisition (lead), Investigation (lead), Methodology (lead), Project administration (lead), Resources (lead),

Software (supporting), Supervision (supporting), Validation (lead), Visualization (lead), Writing – original draft (lead), Writing – review & editing (lead)

Zachary Metzler 0000-0002-1236-8510
Data curation (lead), Formal analysis (supporting), Investigation (supporting), Methodology (supporting), Software (lead), Validation (supporting), Writing – original draft (supporting)

M Coleman Miller 0000-0002-2666-728X
Formal analysis (supporting), Investigation (supporting), Methodology (equal), Software (supporting), Validation (supporting)

Christopher J Collins
Conceptualization (supporting), Data curation (lead), Formal analysis (lead), Investigation (supporting), Methodology (supporting), Software (lead), Supervision (supporting), Validation (supporting), Writing – original draft (supporting)

Clive R Neal 0000-0003-0705-3490
Conceptualization (supporting), Investigation (supporting), Methodology (supporting), Visualization (supporting), Writing – original draft (supporting), Writing – review & editing (supporting)

Slava G Turyshev 0000-0003-4255-9497
Conceptualization (supporting), Investigation (supporting), Methodology (supporting), Visualization (supporting), Writing – original draft (supporting)

Appendix A. Reconstruction of Metric Perturbations from Accelerometer Outputs

In Cartesian coordinates, the along-axis (translational) motions of 2 TMs on each coordinate axis are differenced to measure a diagonal component of the wave, while the cross-axis (rotational) motions of 4 TMs on each coordinate plane are differenced to measure an off-diagonal component of the wave:

$$h_{ii}(t) = \frac{2}{L}\left[x_{+ii}(t) - x_{-ii}(t)\right], \tag{A1a}$$

$$h_{ij}(t) = \frac{1}{L}\left\{\left[x_{+ij}(t) - x_{-ij}(t)\right] - \left[x_{-ji}(t) - x_{+ji}(t)\right]\right\}, i \neq j \tag{A1b}$$

where $x_{\pm ij}(t)$ is displacement of the TM on the $\pm i$ axis along the jth axis and L is the separation between the TMs on each axis. In the baseline LANGO, we have only 4 TMs located on 4 of the 8 vertices of a cube inscribed in the Moon, as shown in figure 3(a). In this tetrahedral geometry, 2 TMs are located at the ends of a diagonal on each of the 6 faces of the cube. We take the mean displacement of each TM pair parallel to the 3 coordinate axes to construct $x_{\pm ij}(t)$. The 6 TM pairs thus constructed are equivalent to 6 TMs located *at the centers of the 6 cube faces*. The baseline of LANGO is *the distance between the TM pairs on the opposite sides of the Moon*, which equals the length of the edge of the cube, $L = \frac{2}{\sqrt{3}}R$. Substituting this into equation (A1), we find

$$h_{xx}(t) = \frac{\sqrt{3}}{R}\left[\frac{x_1(t) + x_3(t)}{2} - \frac{x_2(t) + x_4(t)}{2}\right] \tag{A2a}$$

$$h_{yy}(t) = \frac{\sqrt{3}}{R}\left[\frac{y_1(t) + y_2(t)}{2} - \frac{y_3(t) + y_4(t)}{2}\right], \tag{A2b}$$

$$h_{zz}(t) = \frac{\sqrt{3}}{R}\left[\frac{z_1(t) + z_4(t)}{2} - \frac{z_2(t) + z_3(t)}{2}\right] \tag{A2c}$$

$$h_{xy}(t) = \frac{\sqrt{3}}{2R}\left[\frac{y_1(t) + y_3(t)}{2} - \frac{y_2(t) + y_4(t)}{2}\right] - \left[\frac{x_3(t) + x_4(t)}{2} - \frac{x_1(t) + x_2(t)}{2}\right] \tag{A2d}$$

$$h_{yz}(t) = \frac{\sqrt{3}}{2R}\left[\frac{z_1(t)+z_2(t)}{2} - \frac{z_3(t)+z_4(t)}{2}\right] - \left[\frac{y_2(t)+y_3(t)}{2} - \frac{y_1(t)+y_4(t)}{2}\right] \tag{A2e}$$

$$h_{zx}(t) = \frac{\sqrt{3}}{2R}\left[\frac{x_1(t)+x_4(t)}{2} - \frac{x_2(t)+x_3(t)}{2}\right] - \left[\frac{z_2(t)+z_4(t)}{2} - \frac{z_1(t)+z_3(t)}{2}\right]. \tag{A2f}$$

Now we need to transform the coordinates from the global Cartesian coordinates for GWs to the local north-east-vertical coordinates for each TM. Since the vertical suspension of the TMs is stiffer, we will consider only the horizontal responses of the TMs to GWs. This coordinate transformation simply involves taking a dot product of the Cartesian coordinates with unit vectors in the north direction and the east direction at the appropriate TM. These unit vectors can be found as follows. The unit position vector for TM 1 relative to the center of the Moon is

$$\hat{R}_1 = (x,\, y, z) = \frac{1}{\sqrt{3}}(1,1,1)\,. \tag{A3}$$

The east direction must be perpendicular to this, as well as to the z direction. Therefore, up to a sign, a unit vector in this direction must be

$$\widehat{E} = \left(-\frac{1}{\sqrt{2}}, \frac{1}{\sqrt{2}}, 0\right). \tag{A4}$$

It can be seen by inspection of figure 3(a) that this sign is correct, as this tangent vector points anti-clockwise when viewed from the north pole. Finally, the north unit vector must be perpendicular to both the radial vector and the east unit vector, so can be calculated as a cross product:

$$\widehat{N} = \widehat{R}_1 \times \widehat{E} = \left(-\frac{1}{\sqrt{6}}, -\frac{1}{\sqrt{6}}, \frac{\sqrt{2}}{\sqrt{3}}\right). \tag{A5}$$

Here we see that the sign is correct as the north vector must point in the positive z direction.

We can proceed similarly for the other TMs, and hence the transformation matrices from Cartesian to local north-east coordinates are found to be

$$\begin{pmatrix} x_{1N} \\ x_{1E} \end{pmatrix} = \begin{pmatrix} -\frac{1}{\sqrt{6}} & -\frac{1}{\sqrt{6}} & \frac{\sqrt{2}}{\sqrt{3}} \\ -\frac{1}{\sqrt{2}} & \frac{1}{\sqrt{2}} & 0 \end{pmatrix} \begin{pmatrix} x \\ y \\ z \end{pmatrix} \tag{A6a}$$

$$\begin{pmatrix} x_{2N} \\ x_{2E} \end{pmatrix} = \begin{pmatrix} -\frac{1}{\sqrt{6}} & \frac{1}{\sqrt{6}} & \frac{\sqrt{2}}{\sqrt{3}} \\ -\frac{1}{\sqrt{2}} & -\frac{1}{\sqrt{2}} & 0 \end{pmatrix} \begin{pmatrix} x \\ y \\ z \end{pmatrix} \tag{A6b}$$

$$\begin{pmatrix} x_{3N} \\ x_{3E} \end{pmatrix} = \begin{pmatrix} \frac{1}{\sqrt{6}} & -\frac{1}{\sqrt{6}} & \frac{\sqrt{2}}{\sqrt{3}} \\ \frac{1}{\sqrt{2}} & \frac{1}{\sqrt{2}} & 0 \end{pmatrix} \begin{pmatrix} x \\ y \\ z \end{pmatrix} \tag{A6c}$$

$$\begin{pmatrix} x_{4N} \\ x_{4E} \end{pmatrix} = \begin{pmatrix} \frac{1}{\sqrt{6}} & \frac{1}{\sqrt{6}} & \frac{\sqrt{2}}{\sqrt{3}} \\ \frac{1}{\sqrt{2}} & -\frac{1}{\sqrt{2}} & 0 \end{pmatrix} \begin{pmatrix} x \\ y \\ z \end{pmatrix}. \tag{A6d}$$

Since the TM suspension frequencies will be well below the GW signal frequency, $_0 \ll \omega$, the displacements are related to the accelerations that TMs undergo by

$$\begin{pmatrix} x_{iN} \\ x_{iE} \end{pmatrix} = -\frac{1}{\omega^2}\begin{pmatrix} a_{iN} \\ a_{iE} \end{pmatrix}. \tag{A7}$$

We now transform the coordinates of equations (A2) and substitute equation (A7) to obtain

$$h_{xx}(t) = \frac{\sqrt{3}}{2\sqrt{2}R\omega^2}(a_{1E} - a_{2E} - a_{3E} + a_{4E}) + \frac{1}{2\sqrt{2}R\omega^2}(a_{1N} - a_{2N} - a_{3N} + a_{4N}), \tag{A8a}$$

$$h_{yy}(t) = \frac{\sqrt{3}}{2\sqrt{2}R\omega^2}(-a_{1E} + a_{2E} + a_{3E} - a_{4E}) + \frac{1}{2\sqrt{2}R\omega^2}(a_{1N} - a_{2N} - a_{3N} + a_{4N}), \tag{A8b}$$

$$h_{zz}(t) = \frac{1}{\sqrt{2}R\omega^2}(-a_{1N} + a_{2N} + a_{3N} - a_{4N}) \tag{A8c}$$

$$h_{xy}(t) = \frac{1}{2\sqrt{2}R\omega^2}(a_{1N} + a_{2N} + a_{3N} + a_{4N}), \tag{A8d}$$

$$h_{yz}(t) = \frac{\sqrt{3}}{4\sqrt{2}R\omega^2}(-a_{1E} - a_{2E} + a_{3E} + a_{4E}) + \frac{1}{4\sqrt{2}R\omega^2}(-a_{1N} - a_{2N} + a_{3N} + a_{4N}), \tag{A8e}$$

$$h_{zx}(t) = \frac{\sqrt{3}}{4\sqrt{2}R\omega^2}(a_{1E} - a_{2E} + a_{3E} - a_{4E}) + \frac{1}{4\sqrt{2}R\omega^2}(-a_{1N} + a_{2N} - a_{3N} + a_{4N}), \tag{A8f}$$

where time dependence is implied for the accelerations. This completes the derivation of equation (2).

It may be counter-intuitive that $h_{xy}(t)$ can be constructed with the north acceleration components only. Since the TMs are located on the vertical edges of the cube, which are rotated 45 degrees about the z axis from the coordinate planes, a_{iN} at the TM positions involve motions along the $x \pm y$ directions, combinations of which actually produce rotational motions about the z axis.

Appendix B. Analysis for LANGO-1 Horizontal Acceleration Sensing Circuit

The sensing capacitances are modulated as

$$C_{x-}(x) = C\left(1 + \frac{x}{d}\right)^{-1}, C_{x+}(x) = C\left(1 - \frac{x}{d}\right)^{-1}. \tag{B1}$$

The currents flowing through $C_{x\pm}$ are denoted by $i_{1x\pm}$ and the output current by i_{2x}. We write three circuit equations:

$$\left[\frac{1}{j\omega C}\left(1 + \frac{x}{d}\right) i_{1x-} + j\omega L(i_{1x-} + i_{2x})\right] = V_x \tag{B2}$$

$$\left[\frac{1}{j\omega C}\left(1 - \frac{x}{d}\right) i_{1x+} + j\omega L(i_{1x+} - i_{2x})\right] = V_x \tag{B3}$$

$$j\omega L[(i_{1x+} - i_{2x}) - (i_{1x-} + i_{2x})] - \frac{1}{j\omega C_i} i_{2x} = 0. \tag{B4}$$

We solve equations (B2) and (B3) for $i_{1x\pm}$ and substitute them into equation (B4) to obtain

$$j\omega L\left[\frac{V_x + j\omega L i_{2x}}{\frac{1}{j\omega C}\left(1 - \frac{x}{d}\right) + j\omega L} - \frac{V_x - j\omega L i_{2x}}{\frac{1}{j\omega C}\left(1 + \frac{x}{d}\right) + j\omega L}\right] - \left(2j\omega L + \frac{1}{j\omega C_i}\right) i_{2x} = 0. \tag{B5}$$

Solving equations (B5) for i_{2x}, we find to the first order in x/d:

$$i_{2x} = \frac{1}{\Delta_x}\left(-\frac{V_x}{j\omega L}\frac{x}{d}\right) \tag{B6}$$

where

$$\Delta_x = (1 - \omega^2 LC)\left[1 - \frac{(1 - 2\gamma\omega^2 LC)(1 - \omega^2 LC)}{\gamma(\omega^2 LC)^2}\right] \tag{B7}$$

with $\gamma \equiv C_i/C$. We set $\Delta_x = 0$ to obtain the resonance frequencies of the LC bridge:

$$f_{LC} = \frac{1}{2\pi}\sqrt{\frac{1-\gamma}{LC}}, f'_{LC} = \frac{1}{2\pi}\frac{1}{\sqrt{LC}}. \tag{B8}$$

For JFET, we choose Texas Instruments JFE2140 with noise voltage $e_n = 1.0$ nV Hz$^{-1/2}$, noise current $i_n = 1.6$ fA Hz$^{-1/2}$ over 1–100 kHz and input capacitance $C_i = 13$ pF. This gives $\gamma = 0.13$. The resonance frequency that involves the bridge output is f_{LC}. Substituting the design values of $L = 25$ mH, $C = 100$ pF, we find $f_{LC} = 94$ kHz.

The Johnson noise produced by the resistance in the LC bridge is

$$e_{n,J} = \left(8k_{\mathrm{B}}TQ_{\mathrm{p}}\omega L\right)^{1/2} = 9.0 \times 10^{-8}\ \mathrm{V\ Hz^{-1/2}}. \tag{B9}$$

This dominates over the noise voltage of the amplifier by two orders of magnitude. The noise temperature of the amplifier effectively increases to

$$T_N = \frac{e_{n,J} i_n}{2k_{\mathrm{B}}} = 5.2\ \mathrm{K} \tag{B10}$$

Appendix C. Analysis for LANGO-2 Horizontal Acceleration Sensing Circuit

The sensing capacitances are modulated as

$$C_{x-}(x) = C\left(1 + \frac{x}{d}\right)^{-1}, C_{x+}(x) = C\left(1 - \frac{x}{d}\right)^{-1}. \tag{C1}$$

The current flowing through the transformer primaries are denoted by $i_{1x\pm}$, and the current flowing through the secondaries by i_2. We write three circuit equations:

$$\left[\frac{1}{\mathrm{j}\omega C}\left(1 + \frac{x}{d}\right) + \mathrm{j}\omega L_{t1}\right] i_{1x-} + \mathrm{j}\omega M i_{2x} = V_x \tag{C2}$$

$$\left[\frac{1}{\mathrm{j}\omega C}\left(1 - \frac{x}{d}\right) + \mathrm{j}\omega L_{t1}\right] i_{1x+} - \mathrm{j}\omega M i_{2x} = V_x \tag{C3}$$

$$\mathrm{j}\omega M\left(i_{1x+} - i_{1x-}\right) + \left(2\mathrm{j}\omega L_{t2} + \mathrm{j}\omega L_i\right) i_{2x} = 0 \tag{C4}$$

where $M \equiv k(L_{t1}L_{t2})^{1/2}$ is the mutual inductance between the transformer primary and the secondary, and L_i is the inductance of the SQUID input coil.

We solve equations (C2) and (C3) for $i_{1x\pm}$ and substitute them into equation (C4) to obtain

$$\mathrm{j}\omega M\left[\frac{V_x + \mathrm{j}\omega M i_{2x}}{\frac{1}{\mathrm{j}\omega C}\left(1 - \frac{x}{d}\right) + \mathrm{j}\omega L_{t1}} - \frac{V_x - \mathrm{j}\omega M i_{2x}}{\frac{1}{\mathrm{j}\omega C}\left(1 + \frac{x}{d}\right) + \mathrm{j}\omega L_{t1}}\right] + \mathrm{j}\omega\left(2L_{t2} + L_i\right) i_{2x} = 0. \tag{C5}$$

Solving equation (C5) for i_{2x}, we find to the first order in x/d:

$$i_{2x} = \frac{1}{\Delta_x}\left(-\frac{V_x}{\mathrm{j}\omega M}\frac{x}{d}\right) \tag{C6}$$

where

$$\Delta_x = \left(1 - \omega^2 L_{t1}C\right)\left(1 - \frac{2+\gamma}{2k^2}\frac{1 - \omega^2 L_{t1}C}{\omega^2 L_{t1}C}\right) \tag{C7}$$

with $\gamma \equiv L_i/L_{t2}$. We set $\Delta_x = 0$ to obtain the resonance frequencies of the LC bridge:

$$f_{LC} = \frac{1}{2\pi}\sqrt{\frac{2+\gamma}{2\left(1+k^2\right)+\gamma}}\frac{1}{\sqrt{L_{t1}C}}, f'_{LC} = \frac{1}{2\pi}\frac{1}{\sqrt{L_{t1}C}} \tag{C8}$$

.

The resonance frequency that involves the transformer secondary is f_{LC}. Substituting the design values of $L_{t1} = 20\ \mu$H, $L_{t2} = 5.0\ \mu$H, $C = 100$ pF, and $k^2 = 0.80$, we find $\gamma = 0.36$ and $f_{LC} = 2.7$ MHz.

The noise temperature of the SQUID can be estimated from the input energy resolution of the Magnicon SQUID, $E_A\left(f_{\mathrm{p}}\right) = 280\hbar$ [46]:

$$T_N = \frac{2f_{\mathrm{p}}E_A\left(f_{\mathrm{p}}\right)}{k_{\mathrm{B}}} = 0.017\ \mathrm{K} \tag{C9}$$

References

[1] Abbott B P *et al* (LIGO Scientific Collaboration and Virgo Collaboration) 2016 Observation of gravitational waves from a binary black hole merger *Phys. Rev. Lett.* **116** 061102
[2] Abbott B P *et al* (LIGO Scientific Collaboration and Virgo Collaboration) 2017 GW170817: observation of gravitational waves from a binary neutron star inspiral *Phys. Rev. Lett.* **119** 161101
[3] Reitze D *et al* 2019 Cosmic Explorer: the U.S. contribution to gravitational-wave astronomy beyond LIGO *Bull. Am. Astron. Soc.* **51** 35
[4] Punturo M *et al* 2010 The Einstein telescope: a third-generation gravitational wave observatory *Class. Quantum Grav.* **27** 194002
[5] LISA homepage: www.lisamission.org LISA—the Laser Interferometer Space Antenna
[6] Amaro-Seoane P and Freitag M 2006 Intermediate-mass black holes in colliding clusters: implications for lower frequency gravitational-wave astronomy *Astrophys. J.* **653** L53–L56
[7] Fregeau J M, Larson S L, Miller M C, O'Shaughnessy R and Rasio F A 2006 Observing IMBH-IMBH binary coalescences via gravitational radiation *Astrophys. J.* **646** L135–8
[8] Sesana A 2016 Prospects for multiband gravitational-wave astronomy after GW150914 *Phys. Rev. Lett.* **116** 231102
[9] Lognonne P, Le Feuvre M, Johnson C L and Weber R C 2009 Moon meteoritic seismic hum: steady state prediction *J. Geophys. Res.* **114** E12003
[10] Harms J 2022 Seismic background limitation of lunar gravitational-wave detectors *Phys. Rev. Lett.* **129** 071102
[11] Kawamura S *et al* 2008 The Japanese space gravitational wave antenna—DECIGO *J. Phys.: Conf. Ser.* **122** 012006
[12] Brans C H and Dicke R H 1961 Mach's principle and a relativistic theory of gravitation *Phys. Rev.* **124** 925
[13] Goossens S, Sabaka T J, Wieczorek M A, Neumann G A, Mazarico E, Lemoine F G, Nicholas J B, Smith D E and Zuber M T 2020 High-resolution gravity field models from GRAIL data and implications for models of the density structure of the Moon's crust *J. Geophys. Res. Planets* **125** e2019JE006086
[14] Neal C R 2001 The interior of the Moon: the presence of garnet in the primitive, deep lunar mantle *J. Geophys. Res.* **106** 865–85
[15] NASEM 2011 Vision and Voyages for planetary science in the decade 2013–2022 ISBN 978-0-309-22464-2 (available at: www.nationalacademies.org/publications/13117)
[16] NASEM 2023 Origins, worlds, and life: a decadal strategy for planetary science and astrobiology 2023–2032 ISBN 978-0-309-47578-5 (available at: www.nationalacademies.org/publications/26522)
[17] Neal C R *et al* 2020 The lunar geophysical network, final report to NASA submitted in response to NNH18ZDA001N-PMCS: planetary mission concept studies (available at: https://assets.science.nasa.gov/content/dam/science/psd/planetary-science-division/2024/Lunar-Geophysical-Network.pdf)
[18] Paik H J, Griggs C E, Moody M V, Venkateswara K, Lee H M, Nielsen B A, Majorana E and Harms J 2016 Low-frequency terrestrial tensor gravitational-wave detector *Class. Quantum Grav.* **33** 075003
[19] Paik H J *et al* 2021 Lunar accelerometer network gravitational observatory (LANGO), topical white paper in response to NASA BPS decadal survey 2023–2032
[20] Metzler Z, Collins C J, Paik H J and Shawhan P S 2022 Tetrahedral omnidirectional full-tensor gravitational wave detector *Class. Quantum Grav.* **39** 225012
[21] Paik H J, Collins C J, Shawhan P, Miller M C, Chirenti C, Neal C R and Turyshev S G 2021 Lunar accelerometer network gravitational observatory (LANGO), research campaign white paper in response to NASA BPS decadal survey 2023–2032
[22] de Paula L A N, Norton R S, Paik H J, Schmerr N C, Williamson P R, Chui T C P and Hahn I 2023 High-sensitivity seismometer development for lunar applications *Sensors* **23** 7245
[23] Erwin A, Stone K J, Shelton D, Hahn I, Huie W, de Paula L A N, Schmerr N C, Paik H J and Chui T C P 2021 Electrostatic frequency reduction: a negative stiffness mechanism for measuring dissipation in a mechanical oscillator at low frequency *Rev. Sci. Instrum.* **92** 015101
[24] Langseth M G, Clark S P, Chute J L, Keihm S J and Wechsler A E 1972 The Apollo 15 lunar heat-flow measurement *Earth Moon Planets* **4** 390–410
[25] Moody M V, Chan H A and Paik H J 1986 Superconducting gravity gradiometer for terrestrial and space applications *J. Appl. Phys.* **60** 4308–15
[26] Merkowitz S M and Johnson W 1997 Techniques for detecting gravitational waves with a spherical antenna *Phys. Rev. D* **56** 7513
[27] Majstorović J, Léon Vidal L and Lognonné P 2025 Modeling lunar response to gravitational waves using normal-mode approach and tidal forcing *Phys. Rev. D* **111** 044061
[28] Yan H, Chen X, Zhang J, Zhang F, Wang M and Shao L 2024 Towards a consistent calculation of the lunar response to gravitational waves *Phys. Rev. D* **109** 064092
[29] Cagnoli G, Hough J, DeBra D, Fejer M M, Gustafson E, Rowan S and Mitrofanov V 2000 Damping dilution factor for a pendulum in an interferometric gravitational waves detector *Phys. Lett. A* **272** 39–45
[30] Paik H J, Vol Moody M and Norton R S 2020 SOGRO—Terrestrial full-tensor detector for mid-frequency gravitational waves *Int. J. Mod. Phys. D* **29** 1940001
[31] Cagnoli G, Gammaitoni L, Kovalik J, Marchesoni F and Punturo M 1999 Low-frequency internal friction in clamped-free thin wires *Phys. Lett. A* **255** 230–5
[32] Peterson J R 1993 Observations and modeling of seismic background noise *open-file report 93–322 USGS*
[33] Harms J and Paik H J 2015 Newtonian-noise cancellation in full-tensor gravitational-wave detectors *Phys. Rev. D* **92** 022001
[34] Giganti J J *et al* 1977 Lunar surface gravimeter experiment final report to NASA (University of Maryland)
[35] Paik H J and Venkateswara K Y 2009 Gravitational wave detection on the Moon and the moons of Mars *Adv. Space Res.* **43** 167
[36] Harms J *et al* 2021 Lunar gravitational-wave antenna *Astrophys. J.* **910** 1
[37] Wagoner R V and Paik H J 1976 Multi mode detection of gravitational waves by a sphere *Proc. Accademia Nazionale dei Lincei Int. Symp. on Experimental Gravitation* (*Pavia Italy*) pp 257–65
[38] Johnson W and Merkowitz S M 1993 Truncated icosahedral gravitational wave antenna *Phys. Rev. Lett.* **70** 2367
[39] Coccia E, Lobo J A and Ortega J A 1995 Proposed gravitational wave observatory based on solid elastic spheres *Phys. Rev. D* **52** 3735
[40] Aguiar O D *et al* 2008 The Schenberg spherical gravitational wave detector: the first commissioning runs *Class. Quantum Grav.* **25** 114042
[41] Nunn C *et al* 2020 Lunar seismology: a data and instrumentation review *Space Sci. Rev.* **216** 89

[42] Blanchette-Guertin J-F, Johnson C L and Lawrence J F 2012 Investigation of scattering in lunar seismic coda *J. Geophys. Res.* **117** E06003
[43] Gillet K, Margerin L, Calvet M and Monnereau M 2017 Scattering attenuation profile of the Moon: implications for shallow moonquakes and the structure of the megaregolith *Phys. Earth Planet. Inter.* **262** 28–40
[44] Onodera K, Kawamura T, Tanaka S, Ishihara Y and Maeda T 2021 Numerical simulation of lunar seismic wave propagation: investigation of subsurface scattering properties near Apollo 12 landing site *J. Geophys. Res. Planets* **126** e2020JE006406
[45] Nakamura Y, Dorman J, Duennebier F, Ewing M, Lammlein D and Latham G 1974 High frequency lunar teleseismic events *Proc. 5th Lunar Science Conf* (*Houston Texas*) pp 2883–90
[46] Clarke J 1996 SQUID fundamentals *SQUID Sensors: Fundamentals, Fabrication and Applications* ed H Weinstock (Kluwer Dordrecht) p 32